X-ray magnetic linear dichroism study of field-manipulated canted antiferromagnetism in epitaxial α-Fe$_2$O$_3$ films

Sergey M. Suturin [1,*] Alexander M. Korovin [1] Sergey V. Gastev,[1] Polina A. Dvortsova,[1] Mikhail P. Volkov [1]
Manuel Valvidares,[2] and Nikolai S. Sokolov [1]
[1]*Ioffe Institute, 26 Polytechnicheskaya Street, St. Petersburg 194021, Russia*
[2]*ALBA Synchrotron Light Source, E-08290 Cerdanyola del Vallès, Barcelona, Spain*

This paper describes manipulation of the antiferromagnetic (AFM) moment by external magnetic field in thin epitaxial nanofilms of α-Fe$_2$O$_3$—the iron oxide polymorph known for its canted antiferromagnetism above the Morin temperature. The field-driven rotation of the AFM moment has been detected in thin α-Fe$_2$O$_3$/GaN layers by monitoring the azimuthal field dependence of the x-ray magnetic linear dichroism line shape at L_{23} absorption edge of iron. The presence of the tiny canted ferrimagnetic (FM) moment in α-Fe$_2$O$_3$ makes it possible to manipulate the related AFM moment by applying external magnetic field, monitoring the field-driven rotation of both AFM and FM moments that otherwise can be hardly detected in a nanoscale film by conventional magnetometry. A controllable manipulation of the AFM moment in a thin film by external magnetic field is supposed to be an important keystone for development of the emerging field of AFM spintronics.

I. INTRODUCTION

Antiferromagnetic (AFM) spintronics as a part of modern spintronics utilize different kind of magnetic properties such as ferromagnetic-AFM exchange bias, spin torque currents, and domain wall motion [1]. Within this field, emerging interest in AFM spintronics is motivated by the possibility to potentially utilize AFM materials for energy-saving information storage and processing applications [2–4]. In this view, there exists nowadays a growing interest in the manipulation of the AFM order by electric current [3,5,6] or by interfacial spin-orbit torque [4,7]. While numerous methods have been used so far to study ferromagnetic and ferrimagnetic (FM) materials, the observation of the magnetic effects related to the AFM order is a challenging task due to the absence of the net magnetic moment in an antiferromagnet. Among the techniques able to probe the AFM order or Néel vector are the anisotropic [8] and spin-Hall magnetoresistance [9–11]. The synchrotron method of x-ray magnetic linear dichroism (XMLD) is another powerful tool to study the AFM order through sensitivity of light scattering to magnetism [12–16]. XMLD is defined as the difference between the absorption measured with light polarization parallel and perpendicular to the spin direction. At the iron L edge, this difference is due to the break of symmetry that occurs once an electron is excited from the $2p$ to the $3d$ orbital upon absorption of an x-ray photon. Being sensitive to the square of atomic magnetic moment, the XMLD technique gives access to the AFM order.

Among the many known AFM materials, hematite (α-Fe$_2$O$_3$) is a widely studied prototypical insulating room-temperature (RT) antiferromagnet. Having a simple chemical formula and exhibiting a bunch of nontrivial properties, hematite is considered among others as a candidate material to be used in photoelectrochemical cells for hydrogen generation through water splitting [17,18]. From a magnetic point of view, hematite features as a strongly correlated AFM system due to the electron-electron interaction between Fe^{3+} $3d$ orbitals mediated by octahedral oxygen environment. Above the Morin spin reorientation transition temperature of 260 K, the low symmetry at iron sites allows spin-orbit coupling to cause canting of the moments lying in the basal plane perpendicular to the c axis along one of the twofold axes [19–22].

The magnetic moments of the two α-Fe$_2$O$_3$ sublattices $\mathbf{M}_1$ and $\mathbf{M}_2$ lie in the basal (0001) plane almost antiparallel to each other (Fig. 1). The resulting uncompensated magnetic moment $\mathbf{M} = \mathbf{M}_1 + \mathbf{M}_2$ lies in the same basal plane almost perpendicular to $\mathbf{M}_1$ and $\mathbf{M}_2$ and exactly perpendicular to the AFM moment $\mathbf{L} = \mathbf{M}_1 - \mathbf{M}_2$. The canting angle is a fraction of a degree, and the corresponding very small magnetic moment is below 2 emu/cm^3. In bulk hematite, there is almost no magnetic anisotropy in the basal plane, which means that the resulting magnetic moment $\mathbf{M}$ rotates almost freely around the [001] axis. Below the Morin transition, the anisotropy makes the moments align antiferromagnetically along the c axis. In the nanoscale objects, the transition temperature depends on the particle size [23] and can be totally suppressed due to the presence of impurities and defects. A strong magnetic field along the c axis in the AFM state below the Morin transition is known to induce a spin-flop transition, whereas spins get aligned perpendicular to the c axis [24,25]. The Morin transition significantly affects other physical properties of hematite such as electrical resistance and Hall effect [26–28]. It has been shown in Ref. [29] that the spin Hall magnetoresistance is dominated by the AFM Néel vector rather than by the weak magnetic moment caused by spin canting. The

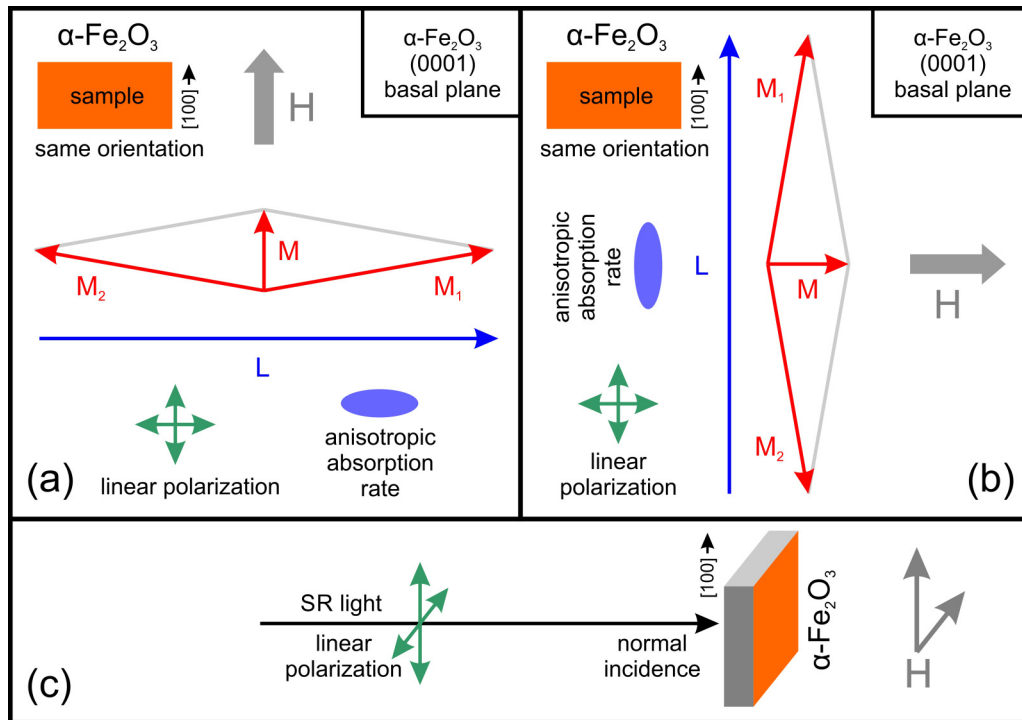*Corresponding author: suturin@mail.ioffe.ru

FIG. 1. A schematic representation of magnetic moments in α-Fe_2O_3. The orientation of resulting ferromagnetic and antiferromagnetic moments in external magnetic field is shown for vertical and horizontal field. The geometry of the normal incidence x-ray magnetic linear dichroism (XMLD) experiment is shown in the bottom image.

electrical switching of the Néel vector in Pt/α-Fe_2O_3 bilayers has been demonstrated recently [30]. Taking advantage of the large XMLD effect associated with the Fe L_{23} edge, it can be effectively applied to α-Fe_2O_3. An XMLD study of the Morin transition in epitaxial α-Fe_2O_3 films doped with Ti, Sn, and Zn is described in Ref. [31]. More recently, magnetic vortex pairs were observed at RT in planar Co/α-Fe_2O_3 films by XMLD photoemission electron microscopy [32]. Being the most thermodynamically stable iron oxide, hematite can be epitaxially grown on many substrates. As was recently demonstrated in Refs. [33–36], the high crystalline quality epitaxial films of hematite and a number of other iron oxide polymorphs can be grown by pulsed laser deposition on a semiconductor GaN surface, opening the way to combine semiconducting and magnetically ordered materials in a hybrid epitaxial heterostructure. In this paper, we have utilized vectorial-field magnetic linear x-ray dichroism and magneto-optical Kerr effect (MOKE) to study magnetic field manipulation of the Néel vector in thin α-Fe_2O_3/GaN films above the Morin temperature.

II. EXPERIMENTAL

The α-Fe_2O_3 single crystal films were grown by means of pulsed laser deposition on the Ga terminated surface of the 3 mkm GaN(0001)/Al_2O_3 templates fabricated by metal organic vapor phase deposition. Following the growth approach described in Ref. [33], iron oxide was deposited from a Fe_2O_3 stoichiometric target ablated by KrF excimer laser. The growth was performed in oxygen at a pressure of 0.02 mbar

at a substrate temperature of 600°C. The crystallinity, epitaxial relations, and defect structure of the grown layers were monitored by *in situ* reflection high-energy electron diffraction (RHEED) reciprocal space three-dimensional mapping [37,38] and x-ray diffraction. As described earlier in Ref. [33], the hematite film grows on GaN with its [001] axis perpendicular to the substrate surface and with the [110] axis parallel to the in-plane GaN [1–10] direction. Figure 2(a) shows typical in-plane and out-of-plane reciprocal space maps obtained by RHEED in α-Fe_2O_3/GaN. The experimentally observed reflections appear exactly where expected for the hematite lattice (the model nodes are shown with circles). The in-plane magnetization curves were measured at RT using the Quantum Design PPMS vibrating sample magnetometer (VSM) and the longitudinal MOKE setup described in Ref. [39]. The x-ray absorption spectroscopy (XAS), x-ray magnetic circular dichroism (XMCD) and XMLD studies have been carried out at the ID32 beamline of ESRF synchrotron (Grenoble, France), the BL7A beamline of KEK PF synchrotron (Tsukuba, Japan), and the BOREAS beamline 29 of ALBA synchrotron (Barcelona, Spain) [40]. The XMCD studies were carried out with the photon incident at 30°, while the XMLD measurements were performed at close to normal incidence. In both cases, the measurements were done in total electron yield (TEY) mode with the magnetic field applied almost in plane of the sample and at RT. The magnetic field was spanned in the range of −2 T to +2 T (ID32 and BL7A beamlines) and could be additionally rotated by 90° in plane of the sample by using a vectorial electromagnet (BL29 beamline).
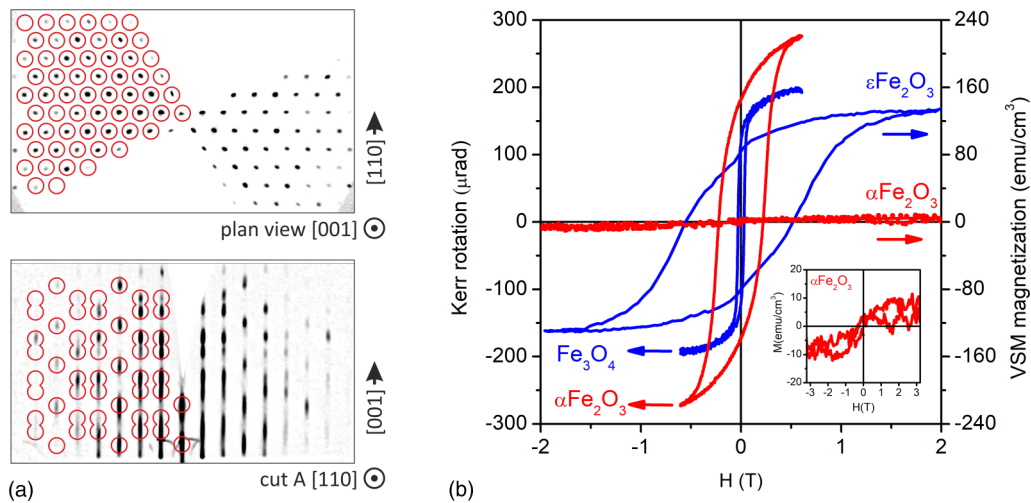
FIG. 2. (a) In-plane (top) and out-of-plane (bottom) reciprocal space maps of α-Fe$_2$O$_3$ film obtained by reflection high-energy electron diffraction (RHEED). The expected positions of reciprocal space nodes in hematite lattice are shown with circles. (b) In-plane magnetization reversal curves measured by longitudinal Kerr effect (left axis) and vibrating sample magnetometer (VSM; right axis) in α-Fe$_2$O$_3$, Fe$_3$O$_4$, and ε-Fe$_2$O$_3$ films on GaN.

III. RESULTS AND DISCUSSION

A. MOKE and VSM studies

The in-plane magnetization reversal in sub-100 nm α-Fe$_2$O$_3$/GaN layers was studied by MOKE (more sensitive) and VSM (more quantitative) to detect the tiny ferromagnetic moment above the Morin temperature. The magnetization loops obtained in an 80 nm α-Fe$_2$O$_3$ film are shown in Fig. 2 together with the curves measured in Fe$_3$O$_4$ and ε-Fe$_2$O$_3$ layers of similar thickness (shown for comparison). Because the canting angle between the AFM aligned magnetic moments in α-Fe$_2$O$_3$ is just a fraction of a degree, the resulting ferromagnetic moment of a sub-100 nm film has appeared too small to be reliably measured by VSM. A magnetization value of below 5 emu/cm^3 was estimated from a rather noisy loop shown in Fig. 2 (negligibly smaller than in the ε-Fe$_2$O$_3$/GaN film of a similar thickness). Remarkably, despite the small net magnetic moment, α-Fe$_2$O$_3$/GaN films showed a well-pronounced Kerr polarization rotation of up to 300 μrad [Fig. 2(b)]. These observations go in line with the anomalously strong magneto-optical effects observed previously in canted antiferromagnets [41] due to the sensitivity of the method to the large Néel vector. Strong linear magnetic birefringence [42] and Kerr rotation [43] comparable with rare earth iron garnets [44] were reported in the early works related to hematite and could be utilized to visualize magnetic domains by polarization microscopy [45]. The unusually high magneto-optical response in materials with weak magnetic moment has been also reported in Ref. [46] for Mn$_3$Sn, rare earth garnets [47], and rare earth ferrites [48].

The field dependence of the MOKE signal was measured in α-Fe$_2$O$_3$/GaN film up to a maximum field of 0.5 T. The shape of the slightly undersaturated minor magnetization loop (Fig. 2) allows estimating coercivity >0.3 T. Such a large coercivity is not typical for the large natural hematite crystals that usually exhibit a much softer magnetic behavior with a typical coercive field of 0.3 to 3 mT. The magnetization in bulk hematite crystals is free to rotate in the basal (001) plane.

In contrast to this, in the large volume samples containing hematite nanoparticles, the coercivity of a few kilo-oersted and saturation field >20 kOe are often observed [49–51]. The main source of the high coercivity in nanoscale objects is believed to be related to magnetoelastic anisotropy associated with the nanoparticle structure, strain, and twinning [52,53]. The high coercivity values in α-Fe$_2$O$_3$/GaN films may be due to the anisotropy related to the columnar structure of the films resulting from the twofold ambiguity of epitaxial relations between trigonal α-Fe$_2$O$_3$ and hexagonal GaN. Encouraged by the high magnetic sensitivity of the visible light magneto-optics, the study of magnetization reversal in α-Fe$_2$O$_3$/GaN films has been continued using synchrotron light x-ray magneto-optical methods.

B. XMCD and XMLD studies

The x-ray absorption technique empowered by XMCD and XMLD is a valuable tool to probe oxidation state, coordination, and magnetization of the 3d elements in magnetically ordered materials. In iron oxides, the ligand field of the oxygen atoms splits the Fe 3d into e_g and t_{2g} manifolds, providing a highly sensitive probe of coordination and magnetization within individual sublattices. The Fe L_3 line shape measured in an 80 nm α-Fe$_2$O$_3$/GaN film is shown in the inset of Fig. 3(a). The deep depression between the main peak at 709.5 eV and the satellite at 708 eV are typical of purely octahedral Fe^{3+} [54–56]. This feature is less pronounced in the $O_h + T_d$ coordinated iron oxides [54,56–58] (see the L_3 line shape in ε-Fe$_2$O$_3$ shown in the inset to Fig. 3 for comparison).

The XMCD across the Fe L_{23} absorption edge was measured in the same α-Fe$_2$O$_3$/GaN film to detect the presence of an uncompensated magnetic moment. At a field of 2 T applied in plane, the difference in absorption of left-right circularly polarized light could hardly be distinguished with the available accuracy [Fig. 3(b)]. Such small XMCD is not surprising considering the very small value of the ferromagnetic moment in α-Fe$_2$O$_3$ above the Morin temperature confirmed earlier by
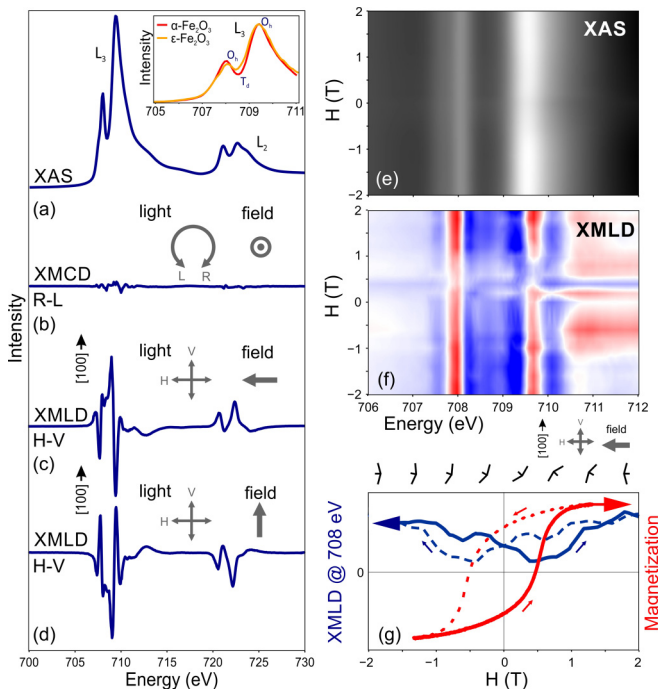
FIG. 3. (a) X-ray absorption spectra measured in α-Fe$_2$O$_3$ films. The inset shows the pure O_h Fe L_3 absorption peak shape compared with $O_h + T_d$ shape measured in ε-Fe$_2$O$_3$ (BL7A). (b) The x-ray magnetic circular dichroism (XMCD) spectrum measured in 2 T in-plane field at 30° incidence with circularly polarized light. The x-ray magnetic linear dichroism (XMLD) spectra measured at BL29 at normal incidence with vertical/horizontal linear polarization for the sample magnetized (c) horizontally and (d) vertically under 2 T applied field. (e) The absorption and (f) XMLD maps (ID32) measured as a function of photon energy and magnetic field. (g) The field-even behavior of XMLD signal at $E = 708.3$ eV. The expected field-odd behavior of magnetization is shown schematically in panel (g) for ease of interpretation.

our VSM studies. Though hard to be detected by XMCD, the response of the **M** vector to the external magnetic field could be successfully tracked down in the α-Fe$_2$O$_3$/GaN films by applying XMLD. The trick was to look at the AFM moment L, which is large and, in a canted antiferromagnet, perpendicular to M. The anisotropy associated with the AFM moment L allows us to detect its direction by the pronounced difference in absorption of linearly polarized light with polarization parallel-perpendicular to L. The XMLD is proportional to $\langle M^2 \rangle$, being therefore sensitive to the orientation but not to the sign of the collinear in-plane magnetization.

In this paper, the field behavior of the canted antiferrimagnetism in α-Fe$_2$O$_3$/GaN films was investigated by measuring Fe L_{23} XMLD as a function of field strength and orientation. Unlike with the circularly polarized light, a very pronounced XMLD difference was found between the spectra measured in linear polarization with polarization parallel and perpendicular to the field [Fig. 3(c)]. To prove that the dichroism has purely magnetic rather than crystallographic origin (natural dichroism), the XMLD spectra were measured twice for mutually perpendicular field directions. The vector field

capability at ALBA XMCD endstation was used to rotate the field direction without moving the sample (see the sketch in Fig. 1). The linear dichroism changed sign [Figs. 3(c) and 3(d)] upon 90° rotation, indicating that the Néel vector is rotated synchronously with the field. Thus, we demonstrate that the direction of the Néel vector, which is perpendicular to the very small uncompensated ferromagnetic moment **M**, can be manipulated by driving M with an external field and monitored by XMLD. The structural part of the linear dichroism, if any, seems negligible compared with the magnetic part.

In addition to studying the magnetization behavior in α-Fe$_2$O$_3$/GaN in a field of a variable orientation, we have investigated the response of the Néel vector to a variable magnetic field of fixed orientation. The maps shown in Figs. 3(e) and 3(f) reflect the shape evolution of XAS and XMLD spectra upon scanning the field from -2 T to $+2$ T. The instrumental dependence of TEY on magnetic field has been compensated in both maps by normalization applied to the nondichroic spectrum regions. To compare behaviors of the ferromagnetic **M** with AFM **L** vectors on the same field scale, the field dependence of XMLD measured at $E = 708.3$ eV is shown in Fig. 3(g). Being taken with an increasing field, the XMLD map corresponds to the lower branch of the magnetization loop. The upper branch is built by inversing the lower branch and is shown with a dashed line. The resulting hysteresis loop has a butterfly shape typical for the quadratic magnetic effects.

The XMLD map is almost symmetrical with respect to $H = +0.5$ T, at which point the net magnetization M presumably crosses zero. At saturation ($H < -1.5$ T or $H > +1.5$ T), where M lies parallel or antiparallel to H (L lies perpendicular to H), the XMLD spectrum shape does not depend on H. At small fields where magnetization switching occurs, the XMLD signal changes fast and behaves even with field. Remarkably, the XMLD signal at 708.3 eV approaches zero at $H_c = +0.5$ T but does not turn negative like in the experiment with the 90° field rotation discussed above. This likely corresponds to the almost equal absorption of horizontally and vertically polarized light observed when the AFM moments are inclined at 45° to polarization. As schematically shown in Fig. 3(g), the orientation of the net magnetic moment changes from negative to positive, and the orientation of the Néel vector is in a qualitative agreement with the shape of the butterfly loop. The corresponding spin reorientation is most likely a combination of a slow rotation followed by abrupt switching, rather than domain wall motion. To account for the observed hysteresis, there must be some anisotropy in the system that prevents magnetic moments to rotate freely. As discussed in the literature [49–51], a large anisotropy (and the related coercive forces) often appears in single-domain granular hematite systems due to magnetoelastic anisotropy associated with internal strains arising from fine particle size as well as from crystal defects such as growth and deformational twinning, antiphase boundaries, and dislocations. For a more detailed analysis of the path which the magnetization vector follows during field reversal, it is suggested to perform a vectorial measurement of magnetic moment, e.g., by longitudinal and transversal MOKE.

IV. CONCLUSIONS

In this paper, we have demonstrated the possibility to manipulate the orientation of the AFM moment in thin epitaxial nanofilms of canted AFM α-Fe$_2$O$_3$ by applying an external magnetic field of variable orientation and strength. In contrast to the large volume hematite crystals, where magnetization behavior can be readily visualized by using conventional techniques such as vibrational and superconducting quantum interference device (SQUID) magnetometry, detecting the very small magnetic moment in a nanoscale α-Fe$_2$O$_3$ film requires a much more sensitive technique. We have demonstrated that visible range MOKE in combination with XMLD are highly appropriate tools to study magnetization in thin films of canted antiferromagnets. The enhanced sensitivity of MOKE to the net magnetization in α-Fe$_2$O$_3$ can be successfully used to acquire magnetization curves helpful for examination of the loop shape, coercivity, and saturation magnetization. The XMCD at the L_{23} edge of iron was shown to be not as sensitive to the ferromagnetic component of magnetization as MOKE. However, linearly polarized x-ray light can be effectively used to detect the orientation of the large AFM moment in α-Fe$_2$O$_3$. The presence of the tiny ferromagnetic moment in a canted antiferromagnet makes it possible to manipulate the AFM moment by applying external magnetic field. The field-driven rotation of the Néel vector in α-Fe$_2$O$_3$ can be tracked down by monitoring the azimuthal field dependence of the XMLD line shape. To our knowledge, XMLD detection of Néel vector rotation above the Morin temperature in hematite has been never reported. The benefit from being able to manipulate the AFM moment by external magnetic field and to monitor it by XMLD or XMLD-photoemission electron microscopy makes it possible to deeper investigate the AFM domain dynamics, which is a keystone in development of the emerging field of AFM spintronics.

[1] O. Bezencenet, D. Bonamy, R. Belkhou, P. Ohresser, and A. Barbier, Origin and Tailoring of the Antiferromagnetic Domain Structure in α-Fe$_2$O$_3$ Thin Films Unraveled by Statistical Analysis of Dichroic Spectromicroscopy (X-Ray Photoemission Electron Microscopy) Images, Phys. Rev. Lett. **106**, 107201 (2011).

[2] T. Jungwirth, X. Marti, P. Wadley, and J. Wunderlich, Antiferromagnetic spintronics, Nat. Nanotechnol. **11**, 231 (2016).

[3] A. H. MacDonald and M. Tsoi, Antiferromagnetic metal spintronics, Philos. Trans. R. Soc. A **369**, 3098 (2011).

[4] T. Moriyama, K. Oda, T. Ohkochi, M. Kimata, and T. Ono, Spin torque control of antiferromagnetic moments in NiO, Sci. Rep. **8**, 14167 (2018).

[5] A. B. Shick, S. Khmelevskyi, O. N. Mryasov, J. Wunderlich, and T. Jungwirth, Spin-orbit coupling induced anisotropy effects in bimetallic antiferromagnets: a route towards antiferromagnetic spintronics, Phys. Rev. B **81**, 212409 (2010).

[6] H. V. Gomonay and V. M. Loktev, Spin transfer and current-induced switching in antiferromagnets, Phys. Rev. B **81**, 144427 (2010).

[7] X. Z. Chen, R. Zarzuela, J. Zhang, C. Song, X. F. Zhou, G. Y. Shi, F. Li, H. A. Zhou, W. J. Jiang, F. Pan, and Y. Tserkovnyak, Antidamping-Torque-Induced Switching in Biaxial Antiferromagnetic Insulators, Phys. Rev. Lett. **120**, 207204 (2018).

[8] A. Azevedo, L. H. Vilela-Leão, R. L. Rodríguez-Suárez, A. F. Lacerda Santos, and S. M. Rezende, Spin pumping and anisotropic magnetoresistance voltages in magnetic bilayers: theory and experiment, Phys. Rev. B **83**, 144402 (2011).

[9] H. Nakayama, M. Althammer, Y.-T. Chen, K. Uchida, Y. Kajiwara, D. Kikuchi, T. Ohtani, S. Geprägs, M. Opel, S. Takahashi, R. Gross, G. E. W. Bauer, S. T. B. Goennenwein, and E. Saitoh, Spin Hall Magnetoresistance Induced by a Nonequilibrium Proximity Effect, Phys. Rev. Lett. **110**, 206601 (2013).

[10] Y.-T. Chen, S. Takahashi, H. Nakayama, M. Althammer, S. T. B. Goennenwein, E. Saitoh, and G. E. W. Bauer, Theory of spin Hall magnetoresistance, Phys. Rev. B **87**, 144411 (2013).

[11] A. Manchon, Spin Hall magnetoresistance in antiferromagnet/normal metal bilayers, Phys. Status Solidi RRL **11**, 1600409 (2017).

[12] M. Blume, Magnetic scattering of x rays (Invited), J. Appl. Phys. **57**, 3615 (1985).

[13] E. Arenholz, G. Van Der Laan, R. V. Chopdekar, and Y. Suzuki, Anisotropic x-ray magnetic linear dichroism at the Fe $L_{2,3}$ edges in Fe$_3$O$_4$, Phys. Rev. B **74**, 094407 (2006).

[14] P. Kuiper, B. G. Searle, P. Rudolf, L. H. Tjeng, and C. T. Chen, X-Ray Magnetic Dichroism of Antiferromagnet Fe$_2$O$_3$: The Orientation of Magnetic Moments Observed by Fe 2p X-Ray Absorption Spectroscopy, Phys. Rev. Lett. **70**, 1549 (1993).

[15] G. Van Der Laan and E. Arenholz, Anisotropic x-ray magnetic linear dichroism its importance for the analysis of soft x-ray spectra of magnetic oxides, Eur. Phys. J. Spec. Top. **169**, 187 (2009).

[16] S.-W. Cheong, M. Fiebig, W. Wu, L. Chapon, and V. Kiryukhin, Seeing is believing: visualization of antiferromagnetic domains, Npj Quantum Mater. **5**, 3 (2020).

[17] K. Sivula, F. Le Formal, and M. Grätzel, Solar water splitting: progress using hematite (α-Fe$_2$O$_3$) photoelectrodes, Chem. Sus. Chem. **4**, 432 (2011).

[18] A. G. Tamirat, J. Rick, A. A. Dubale, W.-N. Su, and B.-J. Hwang, Using hematite for photoelectrochemical water splitting: a review of current progress and challenges, Nanoscale Horizons **1**, 243 (2016).

[19] J. C. Marmeggi, D. Hohlwein, and E. F. Bertaut, Magnetic neutron Laue diffraction study of the domain distribution in α-Fe$_2$O$_3$, Phys. Status Solidi **39**, 57 (1977).

[20] P. Chen, N. Lee, S. McGill, S.-W. Cheong, and J. L. Musfeldt, Magnetic-field-induced color change in α-Fe$_2$O$_3$ single crystals, Phys. Rev. B **85**, 174413 (2012).

[21] I. Dzyaloshinsky, A thermodynamic theory of "weak" ferromagnetism of antiferromagnetics, J. Phys. Chem. Solids **4**, 241 (1958).

[22] T. Moriya, Theory of magnetism of NiF$_2$, Phys. Rev. **117**, 635 (1960).

[23] D. Kubániová, L. Kubíčková, T. Kmječ, K. Závěta, D. Nižňanský, P. Brázda, M. Klementová, and J. Kohout, Hematite: Morin temperature of nanoparticles with different size, J. Magn. Magn. Mater. **475**, 611 (2019).

[24] M. Vasquez-Mansilla, R. Zysler, C. Arciprete, M. Dimitrijewits, D. Rodriguez-Sierra, and C. Saragovi, Annealing effects on structural and magnetic properties of α-Fe$_2$O$_3$ nanoparticles, J. Magn. Magn. Mater. **226–230**, 1907 (2001).

[25] G. J. Muench, S. Arajs, and E. Matijević, The Morin transition in small α-Fe$_2$O$_3$ particles, Phys. Status Solidi **92**, 187 (1985).

[26] A. H. Morrish, G. B. Johnston, and N. A. Curry, Magnetic transition in pure and Ga doped α-Fe$_2$O$_3$, Phys. Lett. **7**, 177 (1963).

[27] C. G. Shull, W. A. Strauser, and E. O. Wollan, Neutron diffraction by paramagnetic and antiferromagnetic substances, Phys. Rev. **83**, 333 (1951).

[28] N. Amin and S. Arajs, Morin temperature of annealed submicronic α-F$_2$O$_3$ particles, Phys. Rev. B **35**, 4810 (1987).

[29] R. Lebrun, A. Ross, O. Gomonay, S. A. Bender, L. Baldrati, F. Kronast, A. Qaiumzadeh, J. Sinova, A. Brataas, R. A. Duine, and M. Kläui, Anisotropies and magnetic phase transitions in insulating antiferromagnets determined by a spin-Hall magnetoresistance probe, Commun. Phys. **2**, 50 (2019).

[30] Y. Cheng, S. Yu, M. Zhu, J. Hwang, and F. Yang, Electrical Switching of Tristate Antiferromagnetic Néel Order in α-Fe$_2$O$_3$ Epitaxial Films, Phys. Rev. Lett. **124**, 027202 (2020).

[31] D. S. Ellis, E. Weschke, A. Kay, D. A. Grave, K. D. Malviya, H. Mor, F. M. F. de Groot, H. Dotan, and A. Rothschild, Magnetic states at the surface of α-Fe$_2$O$_3$ thin films doped with Ti, Zn, or Sn, Phys. Rev. B **96**, 094426 (2017).

[32] F. P. Chmiel, N. Waterfield Price, R. D. Johnson, A. D. Lamirand, J. Schad, G. van der Laan, D. T. Harris, J. Irwin, M. S. Rzchowski, C.-B. Eom, and P. G. Radaelli, Observation of magnetic vortex pairs at room temperature in a planar α-Fe$_2$O$_3$/Co heterostructure, Nat. Mater. **17**, 581 (2018).

[33] S. M. Suturin, A. M. Korovin, S. V. Gastev, M. P. Volkov, A. A. Sitnikova, D. A. Kirilenko, M. Tabuchi, and N. S. Sokolov, Tunable polymorphism of epitaxial iron oxides in the four-in-one ferroic-on-GaN system with magnetically ordered α-, γ-, ε-Fe$_2$O$_3$ and Fe$_3$O$_4$ layers, Phys. Rev. Mater. **2**, 073403 (2018).

[34] V. Ukleev, S. Suturin, T. Nakajima, T. Arima, T. Saerbeck, T. Hanashima, A. Sitnikova, D. Kirilenko, N. Yakovlev, and N. Sokolov, Unveiling structural, chemical and magnetic interfacial peculiarities in ε-Fe$_2$O$_3$/GaN (0001) epitaxial films, Sci. Rep. **8**, 8741 (2018).

[35] V. Ukleev, M. Volkov, A. Korovin, T. Saerbeck, N. Sokolov, and S. Suturin, Stabilization of ε-Fe$_2$O$_3$ epitaxial layer on MgO(111)/GaN via an intermediate γ-phase, Phys. Rev. Mater. **3**, 094401 (2019).

[36] S. M. Suturin, A. M. Korovin, A. A. Sitnikova, D. A. Kirilenko, M. P. Volkov, P. A. Dvortsova, V. A. Ukleev, M. Tabuchi, and N. S. Sokolov, Correlation between crystal structure and magnetism in PLD grown epitaxial films of ε-Fe$_2$O$_3$ on GaN, Sci. Technol. Adv. Mater. **22**, 85 (2021).

[37] S. M. Suturin, A. M. Korovin, V. V. Fedorov, G. A. Valkovsky, M. Tabuchi, and N. S. Sokolov, An advanced three-dimensional RHEED mapping approach to the diffraction study of Co/MnF$_2$/CaF$_2$/Si(001) epitaxial heterostructures, J. Appl. Crystallogr. **49**, 1532 (2016).

[38] S. M. Suturin, V. V Fedorov, A. M. Korovin, G. A. Valkovskiy, S. G. Konnikov, M. Tabuchi, and N. S. Sokolov, A look inside epitaxial cobalt-on-fluorite nanoparticles with three-dimensional reciprocal space mapping using GIXD, RHEED and GISAXS, J. Appl. Crystallogr. **46**, 874 (2013).

[39] B. B. Krichevtsov, S. V Gastev, S. M. Suturin, V. V Fedorov, A. M. Korovin, V. E. Bursian, A. G. Banshchikov, M. P. Volkov, M. Tabuchi, and N. S. Sokolov, Magnetization reversal in YIG/GGG(111) nanoheterostructures grown by laser molecular beam epitaxy, Sci. Technol. Adv. Mater. **18**, 351 (2017).

[40] A. Barla, J. Nicolás, D. Cocco, S. M. Valvidares, J. Herrero-Martín, P. Gargiani, J. Moldes, C. Ruget, E. Pellegrin, and S. Ferrer, Design and performance of boreas, the beamline for resonant x-ray absorption and scattering experiments at the ALBA Synchrotron Light Source, J. Synchrotron Radiat. **23**, 1507 (2016).

[41] A. H. Morrish, Electrical transport and optical properties, in *Canted Antiferromagnetism: Hematite* (World Scientific, Singapore, 1995), pp. 81–85.

[42] H. Le Gall, C. Leycuras, D. Minella, E. G. Rudashewsky, and V. S. Merkoulov, Anomalous evolution of the magnetic and magnetooptical properties of hematite at temperature near and lower than the morin phase transition, Physica B+C **86–88**, 1223 (1977).

[43] G. S. Krinchik and V. E. Zubov, Magnetooptical properties of weak ferromagnets, Zh. Eksp. Teor. Fiz. Pis. Red. **20**, 307 (1974) [JETP Lett. **20**, 137 (1974)].

[44] G. S. Krinchik, A. P. Khrebtov, A. A. Askochenskii, and V. E. Zubov, Surface magnetism of hematite, Zh. Eksp. Teor. Fiz. Pis. Red. **17**, 466 (1973) [JETP Lett. **17**, 335 (1973)].

[45] A. T. Karaev and B. Y. Sokolov, Effect of growth-induced internal stresses on the hematite crystal magnetization in the basal plane, Tech. Phys. **48**, 651 (2003).

[46] T. Higo, H. Man, D. B. Gopman, L. Wu, T. Koretsune, O. M. J. van 't Erve, Y. P. Kabanov, D. Rees, Y. Li, M.-T. Suzuki, S. Patankar, M. Ikhlas, C. L. Chien, R. Arita, R. D. Shull, J. Orenstein, and S. Nakatsuji, Large magneto-optical Kerr effect and imaging of magnetic octupole domains in an antiferromagnetic metal, Nat. Photonics **12**, 73 (2018).

[47] S. Visnovsky, V. Prosser, R. Krishnan, V. Parizek, K. Nitsch, and L. Svobodova, Magnetooptical polar Kerr effect in ferrimagnetic garnets and spinels, IEEE Trans. Magn. **17**, 3205 (1981).

[48] F. J. Kahn, P. S. Pershan, and J. P. Remeika, Ultraviolet magneto-optical properties of single-crystal orthoferrites, garnets, and other ferric oxide compounds, Phys. Rev. **186**, 891 (1969).

[49] Ö. Özdemir and D. J. Dunlop, Hysteresis and coercivity of hematite, J. Geophys. Res. Solid Earth **119**, 2582 (2014).

[50] Y. Yang, J. B. Yi, X. L. Huang, J. M. Xue, and J. Ding, High-coercivity in alpha Fe_2O_3 formed after annealing from Fe_3O_4 nanoparticles, IEEE Trans. Magn. **47**, 3340 (2011).

[51] B. Vallina, J. D. Rodriguez-Blanco, A. P. Brown, L. G. Benning, and J. A. Blanco, Enhanced magnetic coercivity of α-Fe_2O_3 obtained from carbonated 2-line ferrihydrite, J. Nanoparticle Res. **16**, 2322 (2014).

[52] I. Sunagawa and P. J. Flanders, Structural and magnetic studies in hematite single crystals, Philos. Mag. **11**, 747 (1965).

[53] H. Porath and C. B. Raleigh, An origin of the triaxial basal-plane anisotropy in hematite crystals, J. Appl. Phys. **38**, 2401 (1967).

[54] D. H. Kim, H. J. Lee, G. Kim, Y. S. Koo, J. H. Jung, H. J. Shin, J.-Y. Kim, and J.-S. Kang, Interface electronic structures of $BaTiO_3$@X nanoparticles (X = γ-Fe_2O_3, Fe_3O_4, α-Fe_2O_3, and Fe) investigated by XAS and XMCD, Phys. Rev. B **79**, 033402 (2009).

[55] T. J. Regan, H. Ohldag, C. Stamm, F. Nolting, J. Lüning, J. Stöhr, and R. L. White, Chemical effects at metal/oxide interfaces studied by x-ray-absorption spectroscopy, Phys. Rev. B **64**, 214422 (2001).

[56] D. Peak and T. Regier, Direct observation of tetrahedrally coordinated Fe(III) in ferrihydrite, Environ. Sci. Technol. **46**, 3163 (2012).

[57] L. Signorini, L. Pasquini, F. Boscherini, E. Bonetti, I. Letard, S. Brice-Profeta, and P. Sainctavit, Local magnetism in granular iron/iron oxide nanostructures by phase- and site-selective x-ray magnetic circular dichroism, Phys. Rev. B **74**, 014426 (2006).

[58] Y.-C. Tseng, N. M. Souza-Neto, D. Haskel, M. Gich, C. Frontera, A. Roig, M. van Veenendaal, and J. Nogués, Nonzero orbital moment in high coercivity ε-Fe_2O_3 and low-temperature collapse of the magnetocrystalline anisotropy, Phys. Rev. B **79**, 094404 (2009).